

Chronic activation of FXR induced liver growth with tissue-specific targeting Cyclin D1

Weibin Wu, Qing Wu & Xinmei Liu

To cite this article: Weibin Wu, Qing Wu & Xinmei Liu (2019): Chronic activation of FXR induced liver growth with tissue-specific targeting Cyclin D1, Cell Cycle, DOI: [10.1080/15384101.2019.1634955](https://doi.org/10.1080/15384101.2019.1634955)

To link to this article: <https://doi.org/10.1080/15384101.2019.1634955>



View supplementary material [↗](#)



Accepted author version posted online: 21 Jun 2019.



Submit your article to this journal [↗](#)



View Crossmark data [↗](#)

Publisher: Taylor & Francis & Informa UK Limited, trading as Taylor & Francis Group

Journal: *Cell Cycle*

DOI: 10.1080/15384101.2019.1634955

Chronic activation of FXR induced liver growth with tissue-specific targeting Cyclin D1

Running title: FXR induced liver hypertrophy with targeting Ccnd1

Weibin Wu^{a, b, c*}, Qing Wu^d, Xinmei Liu^{a, b, c}

^a The International Peace Maternity and Child Health Hospital, School of Medicine, Shanghai Jiao Tong University, Shanghai, China; ^b Shanghai Key Laboratory of Embryo Original Diseases, Shanghai, China; ^c Shanghai Municipal Key Clinical Specialty, Shanghai, China; ^d Department of Gynecology and Obstetrics, Central Hospital of Minhang District, Shanghai, China.

* Correspondence should be addressed to Weibin Wu, Ph.D., No. 145, Guangyuan Rd., Shanghai 200030, China, Tel: 86-21-64070434, E-mail: wuweibin01@gmail.com.

Abstract

The nuclear receptor (FXR) plays essential roles in maintaining bile acid and lipid homeostasis by regulating diverse target genes. And its agonists were promising agents for treating various liver diseases. Nevertheless, the potential side effect of chronic FXR activation by specific agonists is not fully understood. In this study, we investigated the mechanism of FXR agonist WAY-362450 induced liver enlargement during treating liver diseases. We demonstrated that chronic ingestion of WAY-362450 induced liver hypertrophy instead of hyperplasia in mouse. Global transcriptional pattern was also examined in mouse livers after treatment with WAY-362450 by RNA-seq assay. Through GO and KEGG enrichment analyses, we demonstrated that the expression of Cyclin D1 (*Ccnd1*) among the cell cycle-regulating genes was notably increased in WAY-362450-treated mouse liver. Activation of FXR induced *Ccnd1* expression in hepatocyte in a time-dependent manner *in vivo* and *in vitro*. Through bioinformatics analysis and ChIP assay, we identified FXR as a direct transcriptional activator of *Ccnd1* through binding to a potential enhancer, which was specifically active in livers. We also found active histone acetylation was essential for *Ccnd1* induction by FXR. Thus, our study indicated that activation of FXR induced harmless liver hypertrophy with spatiotemporal modulation of *Ccnd1*. With better understanding of the mechanism of tissue-specific gene regulation by FXR, it is beneficial for development and appropriate application of its specific agonist in preventing

hepatic diseases.

Keywords: Farnesoid x receptor; cyclin D1; WAY-362450; hypertrophy; transcription regulation; histone modification.

Introduction

The farnesoid X receptor (FXR or NR1H4) is a member of the nuclear receptor superfamily, which is constituted by ligand-activated transcription factors and involved in modulation of various fundamental biological processes [1,2]. FXR could be activated by both endogenous ligands (including cholic acid (CA) and chenodeoxycholic acid (CDCA)) and synthetic exogenous agonist with high specificity (such as INT-747, GW4064 and WAY-362450) [3-5]. Studies demonstrated that active FXR played fundamental roles in maintaining bile acid and lipid homeostasis [6,7] through strictly regulating the expression of its target genes, such as small heterodimer partner (*SHP*; *NR0B2*), cholesterol 7 α -hydroxylase (*CYP7A1*), sterol 12 α -hydroxylase (*CYP8B1*), and bile salt export pump (*BSEP*; *ABCB11*) [7-9]. FXR regulates target gene expression through binding to FXR response element (FXRE) within promoter and enhancer regions [10].

FXR is abundantly expressed in liver, gastrointestinal tract, kidney and adrenal gland. Unlike other organs, adult liver maintains unique ability to regrowth/regenerate in response to various injuries primarily by hepatocyte duplication, which is tight controlled by multiple pathways [11,12]. The essential role of FXR in supporting liver regeneration after partial hepatectomy

has been highlighted [13-15]. Nevertheless, it was reported that feeding with excessive bile acid, including CA and CDCA, induces FXR-dependent liver growth by hepatocyte hyperplasia or by hypertrophy, respectively [16]. Liver hypertrophy is also regarded as an adaptation of hepatocytes to increased metabolic demand against toxic drug induced-liver injury [17,18] and is also linked to liver regeneration after partial hepatectomy [19].

Previous studies have characterized FXR as a potential target for the treatment of liver diseases and metabolic disorders [20-23]. In our previous work, we also showed that the FXR agonist WAY-362450 was effective in preventing alcoholic liver disease [21] and intrahepatic cholestasis [24]. However, we observed an unresolved phenomenon that liver size was obviously larger despite recovery from liver injury in WAY-362450 treated mice. Whether chronic ingestion of FXR agonist WAY-362450 induced liver enlargement by potential harmful hyperplasia or by hypertrophy was still unclear. In the present study, we identified that activation of FXR by WAY-362450 promoted liver growth by hypertrophy instead of hyperplasia with direct targeting *Ccnd1* through binding to a tissue-specific enhancer.

Materials and Methods

Animals and Treatments

Wild-type (WT) C57BL/6 mice obtained from Shanghai SLAC laboratory animal Co., Ltd. (Shanghai, China) and FXR knockout (FXR-KO) mice from Jackson Laboratories (Bar Harbor, ME) were maintained in cages with a 12:12 h light-dark cycle. The animal experiments were approved by the Ethics Committee of the International Peace Maternity and Child Health Hospital. All experiments were performed in accordance with ARRIVE (Animal Research: Reporting of *In Vivo* Experiments) guidelines (<http://www.nc3rs.org.uk/arrive-guidelines>) and relevant institutional regulations. All mice received humane care and had free access to water and food. Mouse models for estrogen-induced cholestasis were conducted as described in our previous reports [25]. Briefly, female mice were subcutaneously injected with 5 mg/kg 17 α -ethynylestradiol (Sigma-Aldrich Inc., St. Louis, MO) for four weeks. The synthetic agonist of FXR (WAY-362450, 30 mg/kg body weight) from Selleck Chemicals (Houston, TX) was administered to mice via gavage once a day for up to four weeks. At sacrifice, mice were anesthetized with sodium pentobarbital (75 mg/kg, *ip*). Liver, intestine and kidney tissues were harvested.

RNA Isolation and Reverse Transcription-Quantitative PCR (RT-qPCR)

Isolation of total RNA from tissues and cells was conducted using Trizol reagent (Invitrogen, Carlsbad, CA) according to the manufacturer's instruction.

RNA was reverse transcribed using the PrimeScript RT kit (Takara Biotech, Dalian, China). To detect gene expression, semi-quantitative PCR was performed using Quantitect SYBR Green PCR kit (Qiagen, Hilden, Germany) on the *StepOnePlus* Real-Time PCR System (Applied Biosystems, Foster City, CA). Primers for qPCR assays were included in supplementary material, Table S1. Relative mRNA expression of target genes was calculated using the $2^{-\Delta\Delta Ct}$ method with normalization to β -Actin.

mRNA-seq Assay and Bioinformatics Analysis

Library preparation and high throughput sequencing were conducted as described previously [26]. Briefly, purified RNA was subjected to cDNA libraries construction using the KAPA Stranded RNA-Seq Library Preparation Kit for Illumina Platforms (KAPA biosystems) following the manufacturer's protocol. After purification and quantification, the prepared libraries were subjected to high throughput sequencing on an Illumina HiSeq Xten platforms. Sequential quality control procedures were included. The data were analyzed on the free online platform of Majorbio I-Sanger Cloud Platform (<http://www.i-sanger.com>). Heatmap was plotted using the OmicShare tools (<http://www.omicshare.com/tools>). Gene ontology (GO) and Kyoto Encyclopedia of Genes and Genomes (KEGG) pathway annotations of DEGs were applied using the DAVID Bioinformatics Resources (<https://david.ncifcrf.gov/>). The RNA-seq raw data were deposited to the Sequence Read Archive (<https://www.ncbi.nlm.nih.gov/sra/SRP165945>).

Public datasets

Released public data, including ChIP-seq and DNase-seq data on mouse tissues and HepG2 cells were downloaded from ENCODE (<https://www.encodeproject.org/>) and GEO database. Accession numbers of these data were included in supplementary material, Table S2. These data were reanalyzed and visualized using IGV 2.4 [27] (<http://software.broadinstitute.org/software/igv/>).

Western Blotting Assay

Western blotting assays were conducted as previously described [24]. In brief, tissues and cells were lysed in a RIPA lysis buffer (Beyotime Institute of Biotechnology, Jiangsu, China) with protease inhibitors. Total proteins were separated by SDS-PAGE gels and transferred PVDF membranes (Roche Applied Science). The membranes were incubated with primary antibodies (listed in supplementary material, Table S3) following incubation with HRP-conjugated secondary antibody (Jackson ImmunoResearch, West Grove, PA). The blots were visualized using an enhanced chemiluminescence (ECL) kit (Tiangen Biotech, Beijing, China) on the ImageQuant LAS 4000 mini (GE Healthcare, Piscataway, NJ).

Immunohistochemistry and immunofluorescence Assay

Immunohistochemistry (IHC) and immunofluorescence (IF) assays in the liver tissues were performed as described previously [24]. In brief, tissue sections were subjected to deparaffinization in xylene and antigen retrieval by

boiling in EDTA buffer. Anti-Cyclin D1 antibody (Santa Cruz, Santa Cruz, CA), anti-phospho-histone-H3 (Ser10), a mouse IHC-specific anti-Ki-67 antibody (Cell Signaling Technology) and anti-pan-cadherin (Cell Signaling Technology, Danvers, MA) were applied as primary antibodies, which were incubated overnight at 4°C. For IHC, the tissue sections were incubated with the horseradish peroxidase polymer conjugate (Invitrogen, Carlsbad, CA) and developed with diaminobenzidine chromogen. For IF, Alexa Fluor 488-conjugated Goat anti-rabbit IgG (Invitrogen) was used as the secondary antibody and the nucleus was stained with DAPI. Images were captured using a Leica fluorescence microscope (Leica Microsystems, Wetzlar, Germany).

Chromatin immunoprecipitation (ChIP) assay

ChIP assays with mouse liver tissue using SimpleChIP Plus Enzymatic Chromatin IP Kit were performed according to the manufacturer's protocol (Cell Signaling Technology, Danvers, MA). Briefly, liver tissues were subjected to cross-linking with 1% formaldehyde solution, nuclei preparation and treatment with micrococcal nuclease to digest genomic DNA to a length of approximately 150-900 bp. Furthermore, the digested cross-linked chromatin samples were incubated with the ChIP-grade FXR antibody (Santa Cruz Biotechnology), H3K4me1 and H3K27ac (Cell Signaling Technology) or normal rabbit IgG for immunoprecipitation. After elution and DNA purification, real-time PCR was used to assess target DNA content obtained from immunoprecipitation assay. The results of the ChIP assay in each sample were

shown as proportion of the total input.

Determination of nuclear DNA content in hepatocytes

Nuclear DNA content in mouse hepatocytes was quantified according to a previous report [16]. Briefly, liver sections were deparaffinized, rehydrated and stained with 1 µg/ml Hoechst 33342 (Yeasen Biotech, Shanghai, China). Fluorescent images were acquired under 400x magnifications with a Leica fluorescence microscope (DM2500, Leica Microsystems, Wetzlar, Germany). The fluorescence within the hepatocyte nucleus was identified in images and quantified by CellProfiler Analyst 1.0 software [28].

Cell culture and transfection

HEK293T, HepG2 and Hep3B cells were obtained from the cell bank of Shanghai Institutes for Biological Sciences, Chinese Academy of Sciences (Shanghai, China). HEK293T and HepG2 cells were maintained in Dulbecco's modified Eagle's medium (DMEM, Invitrogen, Carlsbad, CA) containing 10% fetal bovine serum (FBS, Gibco, Grand Island, NY) and antibiotics (100 U/ml penicillin and 0.1 mg/ml streptomycin) at 37°C in 5% CO₂. Hep3B cells were maintained in Eagle's Minimum Essential Medium (EMEM, Invitrogen) supplemented with 10% FBS, 0.11 mg/ml sodium pyruvate and antibiotics. Transient transfection using Lipofectamine 2000 reagent (Invitrogen) was applied according to the manufacturer's protocol.

Plasmid construction and Dual-luciferase assay

Full-length coding regions of FXR and RXR α cDNA were cloned from mouse liver cDNA library and placed into pcDNA3.1 and pcDNA3.0 vectors (Invitrogen, Carlsbad, CA), respectively. DNA fragments containing mouse *Ccnd1* FXRE region (or FXRE region with deletion of putative IR1) were cloned into the pGL3-promoter reporter vector (Promega Corporation, Madison, WI), resulting in pGL3-*Ccnd1*-FXRE and pGL3-*Ccnd1*-FXRE- Δ IR1. One copy of the IR1-type FXR response element (FXRE) from mouse *Nr0b2* gene was cloned into the pGL3-promoter vector (pGL3-*Nr0b2*-FXRE). The putative IR1-type FXRE (CGGTGATTCACCC) from mouse *Ccnd1* gene was also cloned into the pGL3-promoter vector (pGL3-*Ccnd1*-IR1). All the constructs were confirmed by DNA sequencing.

For the dual-luciferase reporter assay, HEK293T cells transfected with pcDNA3.1-FXR, pcDNA3.0-RXR α , pRL-CMV (Promega) and corresponding pGL3-promoter constructs were treated with FXR agonist for next 24 h and subjected to Firefly and Renilla luciferase activity assays. The signals of dual luminescence were recorded in a SpectraMax M3 microplate reader. The relative activity of firefly luciferase was determined by normalizing to Renilla luciferase signals. All experiments were conducted in triplicate.

Mouse Primary hepatocyte isolation and treatment

Mouse primary hepatocytes were isolated using an in situ perfusion collagenase IV method as described previously [29]. Hepatocytes were cultured in 1:1 mixture of DMEM/Ham's F-12 medium (Invitrogen, Carlsbad,

CA) supplemented with 10% FBS. Primary hepatocytes were treated with 2 μ M GW4064 (Sigma-aldrich) or 2 μ M WAY-362450 with or without (+)-JQ1 (MedChem Express, Monmouth Junction, NJ) or C646 (MedChem Express) for several hours prior to gene expression analysis.

Cell growth and cell cycle assays

Cell growth and cell cycle assays were applied as previously described[30]. Briefly, cells were treated with vehicle or FXR agonist for indicated time periods. For cell growth assay, cells were incubated with the Cell Counting Kit-8 (CCK-8) (Dojindo, Kamimashiki-gun Kumamoto, Japan) reagent for 1h and subject to OD450 measurement with a SpectraMax M3 microplate reader (Molecular Devices, Sunnyvale, CA). For cell cycle assay, cells were fixed in ice-cold 70% ethanol before staining with propidium iodide/RNase solution (BD Biosciences, Rockville, MD) and subjected to DNA content determination under a flow cytometer (Beckman Coulter Inc., Miami, FL).

Statistical Analysis

Data are shown as the means \pm SEM. Statistical analysis of numerical data was performed using the GraphPad Prism 5 (GraphPad Software, San Diego, CA) by two-tailed Student's t test and one-way ANOVA followed by Tukey's *post hoc* test for parametric test or Mann-Whitney test for non-parametric test. Fisher's exact test and chi-square test using SPSS 16.0 (SPSS Inc., Chicago, IL) were performed for the analysis of categorical data. Statistical significance was considered as $p < 0.05$.

Results

Chronic ingestion of WAY-362450 induced liver enlargement by hepatocyte hypertrophy in mouse

Previously, we found that administration of WAY-362450 protected against excessive estrogen mediated cholestasis and hepatotoxicity by lowering bile acid level and induction of anti-oxidant response in female mouse [24]. To our surprise, we also found liver size in WAY-362450-treated mouse was noticeably larger than that in vehicle- or estrogen (EE2) alone- treated mice, although liver injury was resolved (Figure 1A-B). As shown, the ratio of liver weight and body weight was increased in wild-type ($p < 0.001$) but not in FXR deficient mouse upon WAY-362450 treatment (Figure 1A). Moreover, WAY-362450 treatment led to cellular and nuclear size increment in hepatocytes. The number of Ki-67 positive hepatocytes was also increased (Figure 1B). Subsequently, we also investigated the effect of WAY-362450 on normal quiescent liver. We demonstrated that liver weight as well as liver/body weight ratio was slightly increased in male mice treated with WAY-362450 for one-week (Figure 1C). Analysis of liver sections revealed that the number of hepatocytes per microscopic field was noticeably reduced with cell size increment in WAY-362450-treated mice (Figure 1D). There were slight increases in Ki67 (*Mki67* gene) expression (Figure 1E) and number of Ki-67-positive hepatocytes (Figure 1F). In addition, gavage with WAY-362450 increased nuclear DNA content hepatocytes (Figure 1G, $p < 0.001$) as

demonstrated by quantitative analysis of Hoechst 33342-stained hepatocyte nuclei. However, the number of mitotic cells (as indicated by positive phospho-histone H3 (serine10) immunostaining [31], Figure 1H) was not obviously changed in WAY-362450-treated mouse. These results suggested that chronic ingestion of WAY-362450 induced FXR-dependent liver hypertrophy in mouse liver.

Activation of FXR by WAY-362450 markedly induced *Ccnd1* expression in mouse liver

To explore the underlying mechanism for FXR induced liver hypertrophy, we examined global gene expression pattern by RNA-seq in mouse livers after WAY-362450 treatment. We found that 346 genes were upregulated and 246 genes were downregulated among a total of 592 differentially expressed genes (DEGs; false discovery rate < 0.05, |fold change| ≥ 2) in WAY-362450-treated mouse compared with and vehicle-treated control (Figure 2A, B). By gene ontology (Figure 2C) and KEGG pathway (Figure 2D) enrichment analyses of DEGs, we found that the cell cycle pathway was also significantly enriched in WAY-362450-treated mouse liver. Moreover, we showed that *Ccnd1* was the most significantly up-regulated and the first-ranked gene among the cell cycle regulating genes (Figure 2E). Subsequently, we applied RT-qPCR assay to verify the RNA-seq result. As shown, FXR was effectively activated by WAY-362450 as demonstrated by significantly upregulated well-established target genes (*Nr0b2* and *Abcb11*) and downregulated *Cyp7a1* (Figure 2F). It

was also validated that the mRNA level of *Ccnd1* among cell cycle genes was significantly upregulated ($p < 0.001$) by WAY-362450 in liver (Figure 2G). We also tested the expression of *Hhex* (also known as HEX) and *Foxm1* (also known as FOXM1b), which were previously reported as FXR target genes in liver growth regulation [14,32]. Whereas, *Hhex* was downregulated ($p < 0.001$) while the expression of *Foxm1* was not significantly changed ($p > 0.05$) in WAY-362450-treated mouse livers (supplementary material, Figure S1). Thus, activation of FXR by WAY-362450 could specially enhance *Ccnd1* expression during induction of hepatocyte hypertrophy in mouse liver *in vivo*.

WAY-362450 enhanced hepatic *Ccnd1* expression time-dependently *in vivo*

To validate the specificity of FXR agonist in *Ccnd1* induction, we tested the mRNA levels of *Nr0b2* and *Ccnd1*, both of which were not obviously changed, in FXR deficient mice livers after treatment with WAY-362450 (Figure 3A). Furthermore, wild-type mice were treated with WAY-362450 for a short period (4h) or 1-3 days. As shown, activation of FXR increased *Nr0b2* and *Ccnd1* expression in mouse liver (Figure 3B-C). Administration of WAY-362450 for one-week (Figure 3D-E) and four weeks (Figure 3-F) led to Cyclin D1 protein increment in mouse livers. Additionally, administration of WAY-362450 enhanced *Nr0b2* while repressed *Ccnd1* expression in both intestine and kidney tissues (Figure 3G). These results further confirmed that activation of FXR might regulate *Ccnd1* expression in time-dependent and tissue-specific

manners.

FXR promoted *Ccnd1* expression time-dependently in hepatocyte *in vitro*.

Subsequently, we analyzed the effect of FXR agonists on the expression of *Ccnd1* in hepatocytes *in vitro*. Mouse primary hepatocytes (mPH) treated with WAY-362450 or GW4064 for 24 h showed abundantly increased *Nr0b2* and *Ccnd1* mRNA levels compared to vehicle-treated controls (Figure 4A). Similarly, incubation with these agonists enhanced *CCND1* expression in the HepG2 (Figure 4B) and Hep3B (Figure 4C) human hepatocellular carcinoma cells. In addition, incubation with the FXR antagonist, Z-guggulsterone, led to decreased expression of *NR0B2* and *CCND1* mRNA (Figure 4D). We further treated HepG2 cells with FXR agonists for various time periods. As expected, activation of FXR induced *NR0B2* and *CCND1* expression in a time-dependent manner in HepG2 cells (Figure 4E). Activation of FXR continually increased *NR0B2* mRNA expression for 72 h. Whereas, the mRNA level of *CCND1* peaked at 24 h and decreased gradually (Figure 4E). The protein level of *CCND1* in HepG2 cells showed a similar expression pattern with WAY-362450 and GW4064 treatment (Figure 4F). However, we did not observe obvious difference in cell cycle progress in mPH (supplementary material, Figure S2A) or cell growth in HepG2 (supplementary material, Figure S2B) cells upon WAY-362450 or GW4064 treatment alone *in vitro*. These data indicated that *Ccnd1* expression was tightly regulated by FXR in a time-dependent manner in

hepatocytes.

FXR regulated *Ccnd1* transcription through direct binding to a downstream IR-1 element

We next explored whether FXR modulated *Ccnd1* expression through transcriptional regulation. Through exploring FXR ChIP-Seq dataset in GEO database (accession: GSE73624), we found that FXR might associate with a downstream region of the mouse *Ccnd1* gene in liver (Figure 5A). The region was also suggested as a potential distal (approximately 10 kb away from transcription start site) active enhancer of *Ccnd1* gene in mouse liver, as indicated by positive histone markers of enhancer, H3K4me1/H3K27ac [33] at the flanking region with assessment of ENCODE epigenomic data (accession: ENCSR854HXZ) [34,35]. Through prediction of FXR binding element by NUBIScan V2.0 (<https://www.nubiscan.unibas.ch>), we found that the region harbored a putative FXR responsive element (a canonical IR-1 consensus sequence), which was conservative in mammals (Figure 5B). By dual-luciferase assay, we confirmed the positive transcriptional regulatory effect of the downstream enhancer and IR-1 element (Figure 5C-D). CHIP-qPCR assays verified that FXR was associated with the IR-1 region downstream the mouse *Ccnd1* gene through direct binding (Figure 5E). Thus, these data indicated that FXR regulated *Ccnd1* expression through direct binding to IR-1 element within a downstream enhancer in mouse liver.

Induction of *Ccnd1* by FXR depended on active histone acetylation

signature

We then explore potential tissue-specific activity of FXR binding region on *Ccnd1* gene. As shown, we demonstrated that WAY-362450 treatment evidently increased the binding of FXR to the IR-1 region in liver instead of intestine (Figure 6A). We also found that positive H3K4me1 and H3K27ac signals were present at the *Ccnd1* enhancer region in liver but not in intestine (Figure 6B). In accord with our findings, the H3K4me1/H3K27ac peaks and the structure accessibility of chromatin at the *Ccnd1* downstream region specially present in mouse liver but absent in intestine, kidney and heart tissues (Figure 6C) with comparing ChIP and DNase-seq (DNase I hypersensitive sites sequencing) data for epigenome in ENCODE database [34,35]. The corresponding downstream region of *CCND1* gene in HepG2 cells also harbored active enhancer markers (H3K4me1/H3K27ac positive) and showed high chromatin accessibility (supplementary material, Figure S3). Furthermore, the binding signals of transcriptional cofactors EP300 and BRD4, which were commonly associated with active enhancer [33], were also observed in HepG2 cells (supplementary material, Figure S3). Subsequently, we tested whether the histone acetylation was involved in FXR-induced *Ccnd1* expression. HepG2 cells and mPH were treated with for histone acetylation inhibitors, BET inhibitor ((+)-JQ1) [36] and EP300/CBP inhibitor (C646) [37]. We showed that the induction effect of WAY-362450 on *CCND1/Ccnd1* and *NR0B2/Nr0b2* expression was almost abrogated by these inhibitors (Figure 6D-E). Hence,

these results indicated that FXR modulated *Ccnd1* transcription through directly binding to an IR-1 element within a tissue-specific enhancer.

Discussion

In this study, we discovered that chronic activation of FXR by specific exogenous agonist WAY-362450 induced liver hypertrophy instead of hyperplasia. FXR regulated *Ccnd1* expression by direct targeting in time-dependent and tissue-specific manners in mouse liver (Figure 6F). In contrast with previous reports, activation of FXR by WAY-362450 did not obviously upregulate the expression of *Hhex*, which was previously identified as FXR target gene during excessive bile acid induced liver hypertrophy [32]. *Foxm1* was also reported as a target gene of FXR during liver regeneration [16]. Although *Foxm1* was slightly upregulated by not reached statistical significance, its expression is still very low in WAY-362450-treated mouse liver (TPM<0.5). The effect of FXR on target gene regulation may depend on affinity of its agonist and microenvironment context.

Although FXR is highly expressed in various tissues, including liver, intestine, kidney and adrenal gland, it is supposed that FXR plays distinct roles in different tissues. A study employing chromatin immunoprecipitation-sequencing (ChIP-seq) to evaluate genome-wide FXR/gene interaction revealed that hepatic and intestinal tissues share only a minor portion of total FXR-binding sites in mice [38]. In particular, genes involved in enterohepatic circulation of bile acid are regulated by FXR in a

liver- and intestine-specific manner [38-41]. Nevertheless, the mechanism of tissue-specific gene regulation by FXR is rarely reported. Gene expression under strict spatiotemporal-regulation is essential to maintain specific cellular identity. Tissue-specific cis-regulatory elements were shown to play important roles in spatiotemporal gene regulation [42]. Here, we showed FXR modulated *Ccnd1* expression tissue-specifically in mouse liver. A possible explanation could be the activity of the downstream enhancer for *Ccnd1* gene was tissue-specific, as indicated by H3K4me1/H3K27ac and chromatin accessibility signals was exclusively present in liver. Indeed, we also showed that FXR agonist did not induce the expression of *Ccnd1* by in both intestine and kidney tissues. A recent study in non-small cell lung cancer also demonstrated that FXR activated Cyclin D1 transcription through binding to an inverted repeat-0 element within *CCND1* promoter [43]. However, we did not observe the binding signal of FXR on *Ccnd1* promoter in mouse liver. Previous reports showed that SHP (NR0B2) could repress *CCND1* transcription in human hepatocellular carcinoma cell lines [44-46]. However, our data suggested that activation of FXR induced *CCND1* expression despite of SHP induction both in mouse and human hepatocytes. Accumulated *Nr0b2* would limit the level of *Ccnd11* induction by FXR. Interestingly, we also found that FXR also induced the expression of a negative regulator in cell cycle progression *Cdkn1a* in mouse liver. Thus, FXR plays comprehensive role in modulation of cell cycle protein expression by FXR depending on cellular

context.

Aberrant bile acid signaling in the absence of hepatic FXR may lead to dysregulated proliferation and malignancy of hepatocytes [46]. In addition, aged FXR-deficient mice spontaneously develop hepatocellular carcinoma and uncontrolled hepatocyte proliferation with dysregulated expression of cell cycle-related genes [47,48]. Thus, FXR may play a comprehensive role in the tight control of cell cycle events and hepatocyte growth. Here, we demonstrated that FXR agonists promoted liver hypertrophy. Although the well characterized positive regulator of G1/S phase Cyclin D1 was substantially upregulated, the expression other negative cell cycle regulated genes (including *Cdkn1a* and *Nr0b2*) was also increased in WAY-362450-treated mice liver under both quiescent and excessive estrogen-induced chronic injury scenarios. Indeed, we demonstrated that a small portion of hepatocytes in WAY-362450-treated mice entered the cell cycle with increased nuclear DNA content. However, most of the hepatocytes were arrested before mitosis. These findings were in accordance with the hypertrophic phenotype of liver growth [16]. Additionally, the findings that FXR agonist alone did not induced hepatocyte proliferation and cell cycle progression *in vitro* also excluded evident mitogenic effect of FXR agonist. Thus, we proposed that FXR agonist WAY-362450 could stimulate liver growth through hepatocyte hypertrophy not hyperplasia.

In addition to its role in metabolic regulation, FXR is also considered as a

hepato-protective factor. Numerous studies have characterized FXR agonists, such as GW4064, WAY-362450 and INT-747, as promising agents for the treatment of liver diseases and metabolic disorders, including alcoholic liver disease, non-alcoholic fatty liver disease, liver fibrosis and intra- or extrahepatic cholestatic disease [20-23], *etc.* Some agonists of FXR are undergoing preclinical and clinical trial. However, the potential side effect of chronic FXR agonist ingestion is still not fully clarified. Whereas, a previous report suggested that chronic activation of FXR in liver and intestine could lead to partial neonatal lethality and growth restriction [49]. In this study, we showed chronic ingestion of WAY-362450 led to liver enlargement. We also demonstrated that WAY-362450 induced benign hypertrophic effect (without obvious hepatocyte proliferation) rather than harmful pathological hyperplasia. We still suggest that correct management of dosage in application of FXR agonist would reduce the risk of potential side effect.

In summary, our study demonstrated that activation of FXR by its specific agonist promoted liver hypertrophy and induced *Ccnd1* expression through direct transcriptional regulation in mouse livers. Furthermore, we identified a novel FXR binding element and a potential enhancer, the activity of which is proposed to be tissue-specific at *Ccnd1* gene. These findings also extend our knowledge on the epigenetic mechanism of FXR-target gene interaction during physiological and pathological conditions. Moreover, it is beneficial for development and appropriate application of specific FXR agonist in preventing

hepatic and metabolic diseases in human with extensive understanding the effect of FXR activation at tissue-specific level.

Disclosure statement

The authors declare no conflict of interest.

Funding

This work was supported by National Natural Science Foundation of China (81501254) and Natural Science Foundation of Shanghai, China (19ZR1462200).

References

1. Forman BM, Goode E, Chen J, *et al.* Identification of a nuclear receptor that is activated by farnesol metabolites. *Cell* 1995; **81**: 687-693.
2. Seol W, Choi HS, Moore DD. Isolation of proteins that interact specifically with the retinoid X receptor: two novel orphan receptors. *Mol Endocrinol* 1995; **9**: 72-85.
3. Maloney PR, Parks DJ, Haffner CD, *et al.* Identification of a chemical tool for the orphan nuclear receptor FXR. *Journal of medicinal chemistry* 2000; **43**: 2971-2974.
4. Pellicciari R, Fiorucci S, Camaioni E, *et al.* 6 α -ethyl-chenodeoxycholic acid (6-ECDCA), a potent and selective FXR agonist endowed with anticholestatic activity. *Journal of medicinal chemistry* 2002; **45**: 3569-3572.
5. Flatt B, Martin R, Wang TL, *et al.* Discovery of XL335 (WAY-362450), a highly potent, selective, and orally active agonist of the farnesoid X receptor (FXR). *Journal of medicinal chemistry* 2009; **52**: 904-907.
6. Laffitte BA, Kast HR, Nguyen CM, *et al.* Identification of the DNA binding specificity and potential target genes for the farnesoid X-activated receptor. *J Biol Chem* 2000; **275**: 10638-10647.
7. Sinal CJ, Tohkin M, Miyata M, *et al.* Targeted disruption of the nuclear receptor FXR/BAR impairs bile acid and lipid homeostasis. *Cell* 2000; **102**: 731-744.
8. Lu TT, Makishima M, Repa JJ, *et al.* Molecular basis for feedback regulation of bile acid synthesis by nuclear receptors. *Molecular cell* 2000; **6**: 507-515.
9. Goodwin B, Jones SA, Price RR, *et al.* A regulatory cascade of the nuclear receptors FXR, SHP-1, and LXR-1 represses bile acid biosynthesis. *Molecular cell* 2000; **6**: 517-526.
10. Massafra V, Pellicciari R, Gioiello A, *et al.* Progress and challenges of selective Farnesoid X Receptor modulation. *Pharmacol Ther* 2018.
11. Yanger K, Knigin D, Zong Y, *et al.* Adult hepatocytes are generated by self-duplication rather than stem cell differentiation. *Cell Stem Cell* 2014; **15**: 340-349.
12. Borude P, Edwards G, Walesky C, *et al.* Hepatocyte-specific deletion of farnesoid X receptor

- delays but does not inhibit liver regeneration after partial hepatectomy in mice. *Hepatology* 2012; **56**: 2344-2352.
13. Huang W, Ma K, Zhang J, *et al.* Nuclear receptor-dependent bile acid signaling is required for normal liver regeneration. *Science* 2006; **312**: 233-236.
 14. Chen WD, Wang YD, Zhang L, *et al.* Farnesoid X receptor alleviates age-related proliferation defects in regenerating mouse livers by activating forkhead box m1b transcription. *Hepatology* 2010; **51**: 953-962.
 15. Merlen G, Ursic-Bedoya J, Jourdainne V, *et al.* Bile acids and their receptors during liver regeneration: "Dangerous protectors". *Mol Aspects Med* 2017; **56**: 25-33.
 16. Milona A, Owen BM, van Mil S, *et al.* The normal mechanisms of pregnancy-induced liver growth are not maintained in mice lacking the bile acid sensor Fxr. *Am J Physiol Gastrointest Liver Physiol* 2010; **298**: G151-158.
 17. Dai X, De Souza AT, Dai H, *et al.* PPARalpha siRNA-treated expression profiles uncover the causal sufficiency network for compound-induced liver hypertrophy. *PLoS Comput Biol* 2007; **3**: e30.
 18. Hall AP, Elcombe CR, Foster JR, *et al.* Liver hypertrophy: a review of adaptive (adverse and non-adverse) changes--conclusions from the 3rd International ESTP Expert Workshop. *Toxicol Pathol* 2012; **40**: 971-994.
 19. Miyaoka Y, Ebato K, Kato H, *et al.* Hypertrophy and unconventional cell division of hepatocytes underlie liver regeneration. *Curr Biol* 2012; **22**: 1166-1175.
 20. Verbeke L, Mannaerts I, Schierwagen R, *et al.* FXR agonist obeticholic acid reduces hepatic inflammation and fibrosis in a rat model of toxic cirrhosis. *Sci Rep* 2016; **6**: 33453.
 21. Wu W, Zhu B, Peng X, *et al.* Activation of farnesoid X receptor attenuates hepatic injury in a murine model of alcoholic liver disease. *Biochem Biophys Res Commun* 2014; **443**: 68-73.
 22. Zhang S, Wang J, Liu Q, *et al.* Farnesoid X receptor agonist WAY-362450 attenuates liver inflammation and fibrosis in murine model of non-alcoholic steatohepatitis. *J Hepatol* 2009; **51**: 380-388.
 23. Liu Y, Binz J, Numerick MJ, *et al.* Hepatoprotection by the farnesoid X receptor agonist GW4064 in rat models of intra- and extrahepatic cholestasis. *The Journal of clinical investigation* 2003; **112**: 1678-1687.
 24. Wu WB, Xu YY, Cheng WW, *et al.* Agonist of farnesoid X receptor protects against bile acid induced damage and oxidative stress in mouse placenta--a study on maternal cholestasis model. *Placenta* 2015; **36**: 545-551.
 25. Fiorucci S, Clerici C, Antonelli E, *et al.* Protective effects of 6-ethyl chenodeoxycholic acid, a farnesoid X receptor ligand, in estrogen-induced cholestasis. *The Journal of pharmacology and experimental therapeutics* 2005; **313**: 604-612.
 26. Zeng W, Liu Z, Liu X, *et al.* Distinct Transcriptional and Alternative Splicing Signatures of Decidual CD4(+) T Cells in Early Human Pregnancy. *Front Immunol* 2017; **8**: 682.
 27. Thorvaldsdottir H, Robinson JT, Mesirov JP. Integrative Genomics Viewer (IGV): high-performance genomics data visualization and exploration. *Brief Bioinform* 2013; **14**: 178-192.
 28. Carpenter AE, Jones TR, Lamprecht MR, *et al.* CellProfiler: image analysis software for identifying and quantifying cell phenotypes. *Genome Biol* 2006; **7**: R100.
 29. Ryu D, Oh KJ, Jo HY, *et al.* TORC2 regulates hepatic insulin signaling via a mammalian

- phosphatidic acid phosphatase, LIPIN1. *Cell metabolism* 2009; **9**: 240-251.
30. Wu W, Wang Y, Xu Y, *et al.* Dysregulated activation of c-Src in gestational trophoblastic disease contributes to its aggressive progression. *Placenta* 2014; **35**: 824-830.
 31. Tetzlaff MT, Curry JL, Ivan D, *et al.* Immunodetection of phosphohistone H3 as a surrogate of mitotic figure count and clinical outcome in cutaneous melanoma. *Mod Pathol* 2013; **26**: 1153-1160.
 32. Xing X, Burgermeister E, Geisler F, *et al.* Hematopoietically expressed homeobox is a target gene of farnesoid X receptor in chenodeoxycholic acid-induced liver hypertrophy. *Hepatology* 2009; **49**: 979-988.
 33. Shlyueva D, Stampfel G, Stark A. Transcriptional enhancers: from properties to genome-wide predictions. *Nat Rev Genet* 2014; **15**: 272-286.
 34. Rosenbloom KR, Sloan CA, Malladi VS, *et al.* ENCODE data in the UCSC Genome Browser: year 5 update. *Nucleic Acids Res* 2013; **41**: D56-63.
 35. Yue F, Cheng Y, Breschi A, *et al.* A comparative encyclopedia of DNA elements in the mouse genome. *Nature* 2014; **515**: 355-364.
 36. Booth CAG, Barkas N, Neo WH, *et al.* Ezh2 and Runx1 Mutations Collaborate to Initiate Lympho-Myeloid Leukemia in Early Thymic Progenitors. *Cancer Cell* 2018; **33**: 274-291 e278.
 37. Lasko LM, Jakob CG, Edalji RP, *et al.* Discovery of a selective catalytic p300/CBP inhibitor that targets lineage-specific tumours. *Nature* 2017; **550**: 128-132.
 38. Thomas AM, Hart SN, Kong B, *et al.* Genome-wide tissue-specific farnesoid X receptor binding in mouse liver and intestine. *Hepatology* 2010; **51**: 1410-1419.
 39. Dawson PA, Hubbert M, Haywood J, *et al.* The heteromeric organic solute transporter alpha-beta, Ostalpha-Ostbeta, is an ileal basolateral bile acid transporter. *J Biol Chem* 2005; **280**: 6960-6968.
 40. Kong B, Wang L, Chiang JY, *et al.* Mechanism of tissue-specific farnesoid X receptor in suppressing the expression of genes in bile-acid synthesis in mice. *Hepatology* 2012; **56**: 1034-1043.
 41. Zhu Y, Li F, Guo GL. Tissue-specific function of farnesoid X receptor in liver and intestine. *Pharmacol Res* 2011; **63**: 259-265.
 42. Russo M, Natoli G, Ghisletti S. Housekeeping and tissue-specific cis-regulatory elements: Recipes for specificity and recipes for activity. *Transcription* 2018; **9**: 177-181.
 43. You W, Chen B, Liu X, *et al.* Farnesoid X receptor, a novel proto-oncogene in non-small cell lung cancer, promotes tumor growth via directly transactivating CCND1. *Sci Rep* 2017; **7**: 591.
 44. Zhang Y, Xu P, Park K, *et al.* Orphan receptor small heterodimer partner suppresses tumorigenesis by modulating cyclin D1 expression and cellular proliferation. *Hepatology* 2008; **48**: 289-298.
 45. Ohno T, Shirakami Y, Shimizu M, *et al.* Synergistic growth inhibition of human hepatocellular carcinoma cells by acyclic retinoid and GW4064, a farnesoid X receptor ligand. *Cancer Lett* 2012; **323**: 215-222.
 46. Kong B, Zhu Y, Li G, *et al.* Mice with hepatocyte-specific FXR deficiency are resistant to spontaneous but susceptible to cholic acid-induced hepatocarcinogenesis. *Am J Physiol Gastrointest Liver Physiol* 2016; **310**: G295-302.

47. Kim I, Morimura K, Shah Y, *et al.* Spontaneous hepatocarcinogenesis in farnesoid X receptor-null mice. *Carcinogenesis* 2007; **28**: 940-946.
48. Yang F, Huang X, Yi T, *et al.* Spontaneous development of liver tumors in the absence of the bile acid receptor farnesoid X receptor. *Cancer Res* 2007; **67**: 863-867.
49. Cheng Q, Inaba Y, Lu P, *et al.* Chronic activation of FXR in transgenic mice caused perinatal toxicity and sensitized mice to cholesterol toxicity. *Mol Endocrinol* 2015; **29**: 571-582.

Figure 1. WAY-362450 promoted liver growth by induction of hepatocyte

hypertrophy in mouse. (A-B) Wild type (WT) or FXR deficient (FXR-KO) mice (female; 8-10-week-old) treated with 17 α -ethynylestradiol (EE2; 5 mg/kg, s.c.) were simultaneously gavaged with (EE2-WAY) or without (EE2-Veh) WAY-362450 for four weeks. (A) The ratios of liver / body weight in each group were shown; (B) Representative images were shown for staining with H&E (upper panels) or immunohistochemistry of Ki67 (lower panels) in WT liver tissues (Original magnification 200 x, bar: 100 μ m). (C-H) WT mice (male; 8 weeks old) were administrated with either vehicle (Veh) or WAY-362450 (WAY) once daily for one-week. (C) The liver weight and ratios of liver/body weight in vehicle (Veh) or WAY-362450 (WAY)-treated mice were shown; (D) Plasma membrane of hepatocytes was immuno-stained by pan-cadherin (red), and the nucleus was stained by DAPI (blue). Original magnification 200 x, bar: 25 μ m. (E) The number of hepatocytes per microscope field. (F) The expression of *Mki67* and *Pcna* in liver tissues was determined by RT-qPCR assay. (G) Representative images are shown for immunohistochemistry staining of Ki-67 in liver tissues from vehicle- or WAY-362450-treated mice; Original magnification 200 x, bar: 100 μ m for upper panel. The proportions of Ki67- positive hepatocytes in livers

of vehicle or WAY-362450 treated mice were shown in right panel. (G) Nuclear DNA content in hepatocytes was semi-quantified in vehicle and WAY-362450-treated mice; 1,500 nuclei were considered in hepatocytes. (H) The proportions of mitotic figure (as indicated by phospho-histone-H3 (Ser10) positive hepatocytes) in livers of vehicle or WAY-362450 treated mice were shown. (Data are represented as mean \pm SEM; * $p < 0.05$, *** $p < 0.001$, ns: not significant ($p > 0.05$))

Figure 2. Activation of FXR by WAY-362450 markedly induced *Ccnd1* expression in mouse liver. Male mice (8 weeks old) were administrated with either vehicle (Veh) or WAY-362450 (WAY) once daily for one-week. Gene expression pattern in mouse livers were analyzed by RNA-seq assay. (A-B) Volcano plot (A) and heatmap (B) for identification of differentially expressed genes (DEGs, |fold change| ≥ 2 , FDR < 0.05 ; $n=3$ in each group) in mouse liver tissues upon WAY-362450 treatment. (C-D) Gene ontology (GO; C) and KEGG pathway (D) enrichment analysis of DEGs in mouse liver after WAY-362450 treatment was shown ($p < 0.05$). (E) The expression of cell cycle-regulating genes in the RNA-seq data was displayed as a heatmap. (F-G) Liver tissues from mice treated with vehicle or WAY-362450 were subjected to RT-qPCR assays for determination mRNA expression of the well-known FXR target genes (*Nr0b2*, *Abcb11* and *Cyp7a1*) and cell cycle genes (*Ccna2*, *Ccnb1*, *Ccnb2*, *Ccnd1*, *Ccne1*, *Cdkn1a*, *Cdkn1b*, *Cdkn2c*, *Cdk1*, *Cdk2*, *Cdk4* and *Cdk6*). ($n=8$; * $p < 0.05$, *** $p < 0.001$; ns, not significant)

Figure 3. WAY-362450 enhanced *Ccnd1* expression time-dependently in mouse livers. (A) FXR deficient mice were treated with either vehicle (Veh) or WAY-362450 (WAY) for 24 h. The mRNA levels of *Nr0b2* and *Ccnd1* in mouse livers were determined by RT-qPCR (n=6 each). (B) The mRNA levels of *Nr0b2* and D-type cyclin family members (*Ccnd1*, *Ccnd2* and *Ccnd3*) in mouse livers after WAY-362450 treatment for 4h were determined by RT-qPCR (n=6). (C) The hepatic mRNA levels of *Nr0b2* and *Ccnd1* in wild-type male mice treated with vehicle or WAY-362450 for 1-3 days were determined by RT-qPCR. (D-E) Male mice were treated with WAY-362450 for one-week. (D) Representative images are shown for immunohistochemistry staining of Cyclin D1 in liver tissues from vehicle- or WAY-362450-treated mice. Original magnification 200 x, bar: 100 μ m for upper panel. (E) The protein level of Cyclin D1 in mouse livers was determined by Western blot assay. Densitometric analysis of Cyclin D1 band density with normalization to β -Actin was shown in lower panel. (F) The protein level of Cyclin D1 in female mouse livers treated with WAY-362450 for four weeks was determined by Western blot. (G) The expression levels of *Nr0b2* and *Ccnd1* in intestine and kidney tissues from mice treated with vehicle or WAY-362450 for one-week were determined by RT-qPCR. (Mean \pm SEM, *** p < 0.001; ns, not significant)

Figure 4. FXR promoted *Ccnd1* expression time-dependently in hepatocyte *in vitro*. (A-C) Mouse primary hepatocytes (A; mPH) and human hepatocellular carcinoma cell lines HepG2 (B) and Hep3B (C) were treated

with DMSO (Veh), WAY-362450 (WAY, 2 μ M) or GW4064 (GW, 2 μ M) for 24 h. (D) HepG2 cells were treated with an FXR antagonist (z-guggulsterone, 20 μ M) for 24 h. The mRNA expression levels of *Nr0b2* (or *NR0B2*) and *Ccnd1* (or *CCND1*) were determined by RT-qPCR. (E) HepG2 cells treated with DMSO, WAY-362450 (2 μ M) or GW4064 (2 μ M) were harvested at indicated time points and subjected to RT-qPCR analysis of *NR0B2* and *CCND1* mRNA levels. (F) Western blot analysis of *CCND1* protein levels in 2 μ M WAY-362450-treated HepG2 cells for 12, 24, 48 and 72 h. Densitometric analysis of Western blot result with normalization to β -Actin was shown in right panel. (Mean \pm SEM; * p < 0.05, ** p < 0.01, *** p < 0.001)

Figure 5. FXR regulates *Ccnd1* transcription through direct binding to a downstream potential enhancer. (A) Public data, including FXR ChIP-seq (GEO: GSE73624), and H3K4me1, H3K4me3 and H3K27ac ChIP-seq (ENCODE: ENCSR854HXZ) on adult mouse livers were analyzed for potential FXR binding sites and enhancer signature on mouse *Ccnd1* gene. The results were exhibited on IGV 2.4 software. (B) Sequence alignment of the putative FXR responsive element (inverted repeat-1, IR-1) downstream *Ccnd1* gene in mouse, rat, guinea pig, dog, horse, bushbaby, marmoset, rhesus, chimp, orangutan, and human. The consensus sequence in IR-1 elements were shown in red. (C) HEK293T cells were transfected with constructs containing FXR response element (FXRE)-approximal region (*Ccnd1*-FXRE) in *Ccnd1*, *Ccnd1*-FXRE region with IR1 deletion (*Ccnd1*-FXRE- Δ IR1), or *Ccnd1* IR1 core

element (*Ccnd1*-IR1). The construct containing the mouse *Nr0b2* FXRE-containing region was used as a positive control (*Nr0b2*-FXRE). After treatment with vehicle (Veh) or WAY-362450 (WAY), the cells were subjected to dual-luciferase reporter assays. (D) HEK-293T Cells transfected with constructs containing *Ccnd1*-FXRE or the FXR response element (FXRE) from the mouse *Nr0b2* gene (*Nr0b2*-FXRE) were treated with 2 μ M WAY-362450 for indicated time period. The activity of IR1 element of *Ccnd1* was determined by dual-luciferase reporter assay. (E) A chromatin immunoprecipitation-quantitative PCR (ChIP-qPCR) assay was conducted using liver tissues from vehicle or WAY-362450-treated mice (n=3 each). ChIP signals are expressed as the ratio of immunoprecipitated DNA to the total input chromatin. A region of the *Actb* promoter was used as a negative control. The proximal region of the *Nr0b2* promoter containing FXRE was used as the positive control. (Mean \pm SEM; * p < 0.05, ** p < 0.01, *** p < 0.001; ns, not significant)

Figure 6. The signature of downstream enhancer of *Ccnd1* was tissue-specific and developmental stage-dependent in liver. (A) ChIP-qPCR analysis of FXR binding on *Ccnd1* gene in vehicle or WAY-362450 treated liver and intestine tissues (n=4). (B) The levels of H3K4me1 and H3K27ac at FXR binding region of *Ccnd1* gene in liver and intestine tissues (n=4) were examined. (C) ChIP-seq data of histone modifications (H3K4me1, H3K4me3, H3K27ac and H3K27me3) and chromatin accessibility (DNase-seq)

on *Ccnd1* gene from ENCODE were visualized using IGV 2.4 software. Data on liver, small intestine, kidney and heart tissues in adult mouse (8 week) were analyzed. (D-E) Mouse primary hepatocytes (D) and HepG3 cells (E) were treated with 2 μ M WAY-362450 with or without 3 μ M (+)-JQ1 and 10 μ M C646 for 4 hours. The mRNA levels of *NR0B2* and *CCND1* genes were determined by RT-qPCR assay. (Mean \pm SEM, *** p < 0.001) (F) Schematic diagram for FXR agonist in induction of liver and hepatocyte hypertrophy by regulating *Ccnd1* expression through binding to a potential enhancer region (H3K4me1/H3K27ac positive and H3K4me3 negative). Red oval, H3K4me1; Green oval, H3K27ac; Blue oval, H3K4me3.

Accepted Manuscript

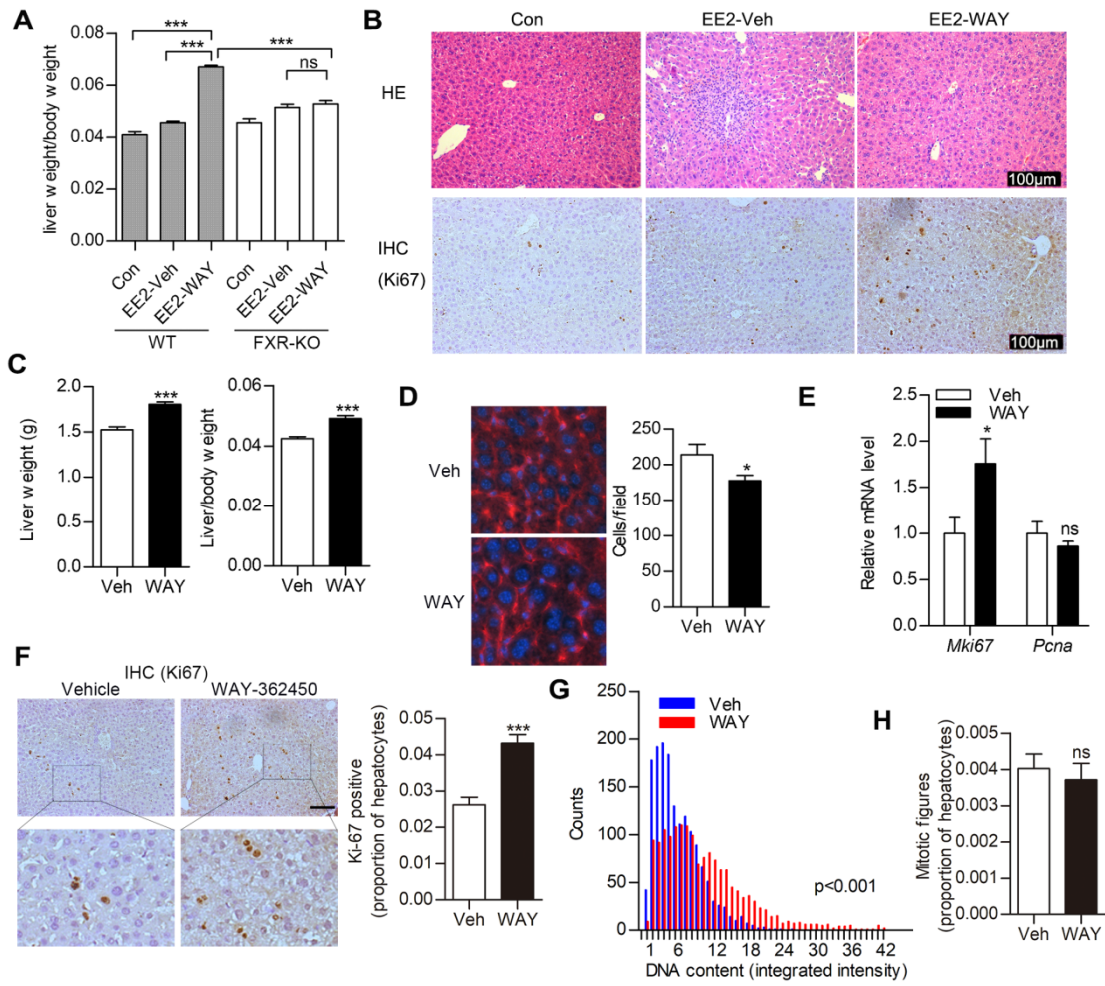
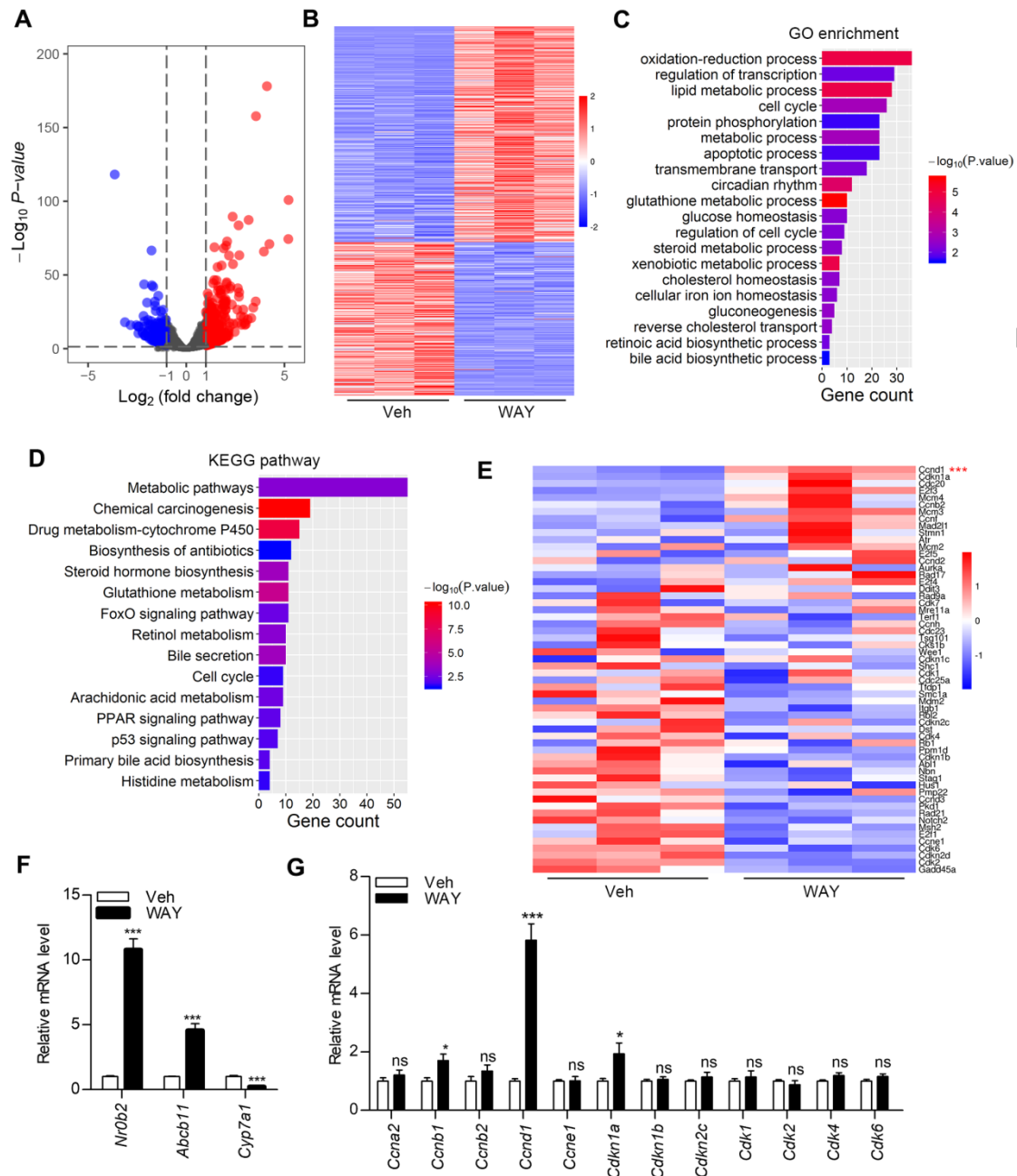


Figure 1

Accepted



ACC
Figure 2

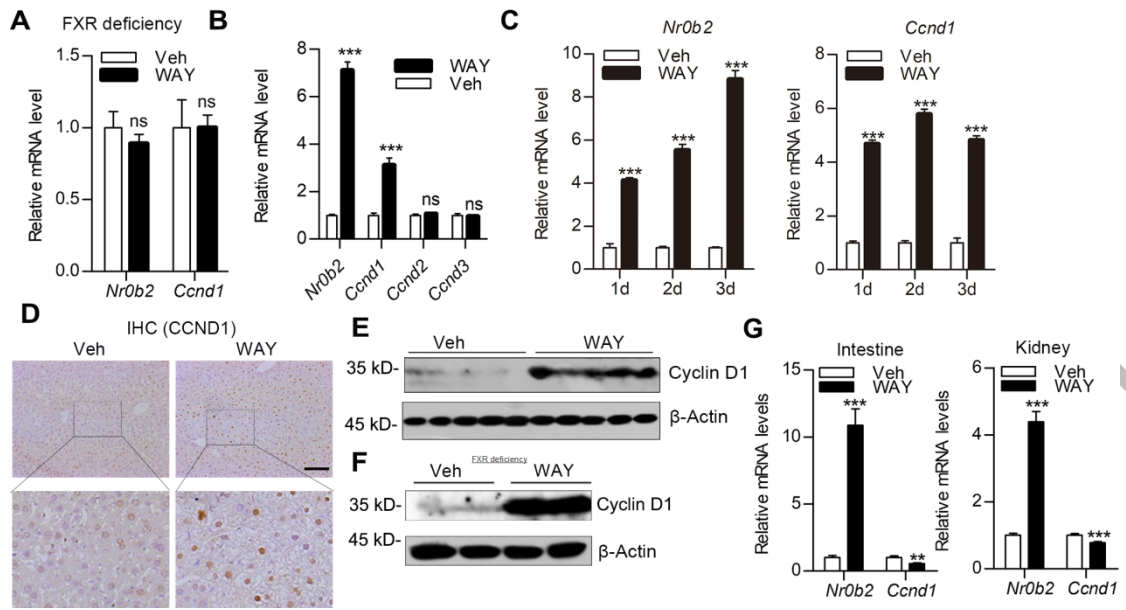


Figure 3

Accepted Manuscript

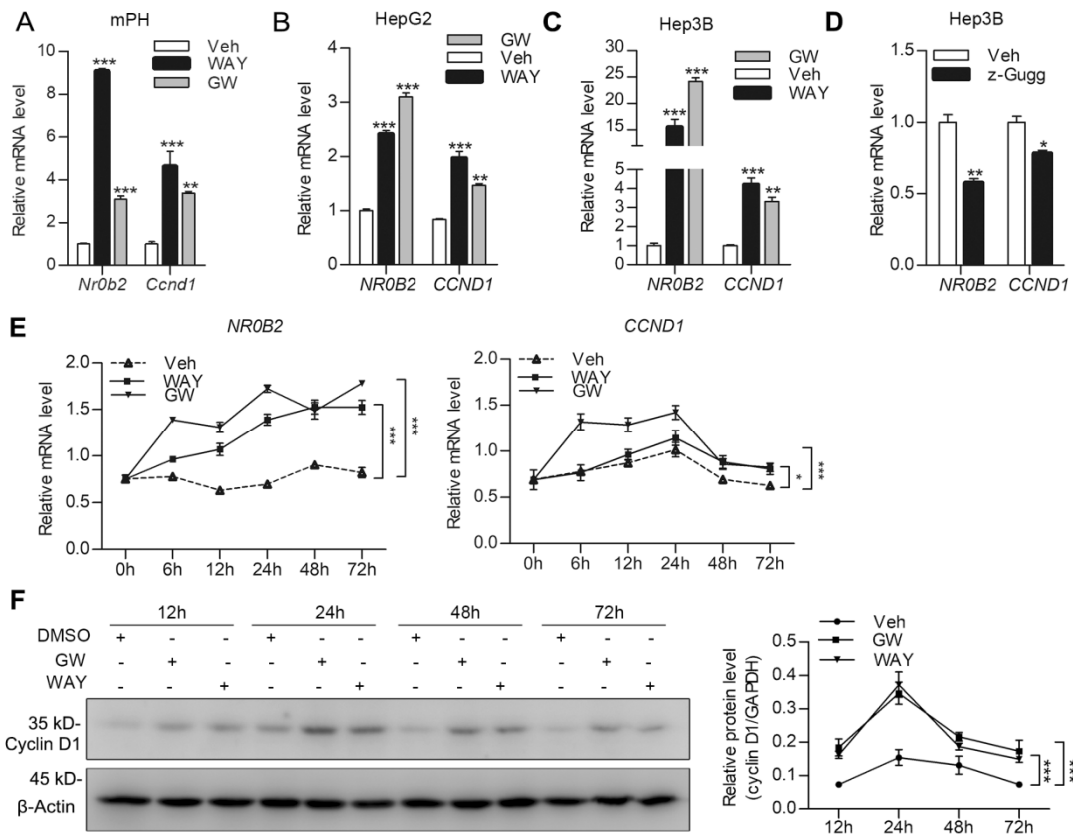


Figure 4

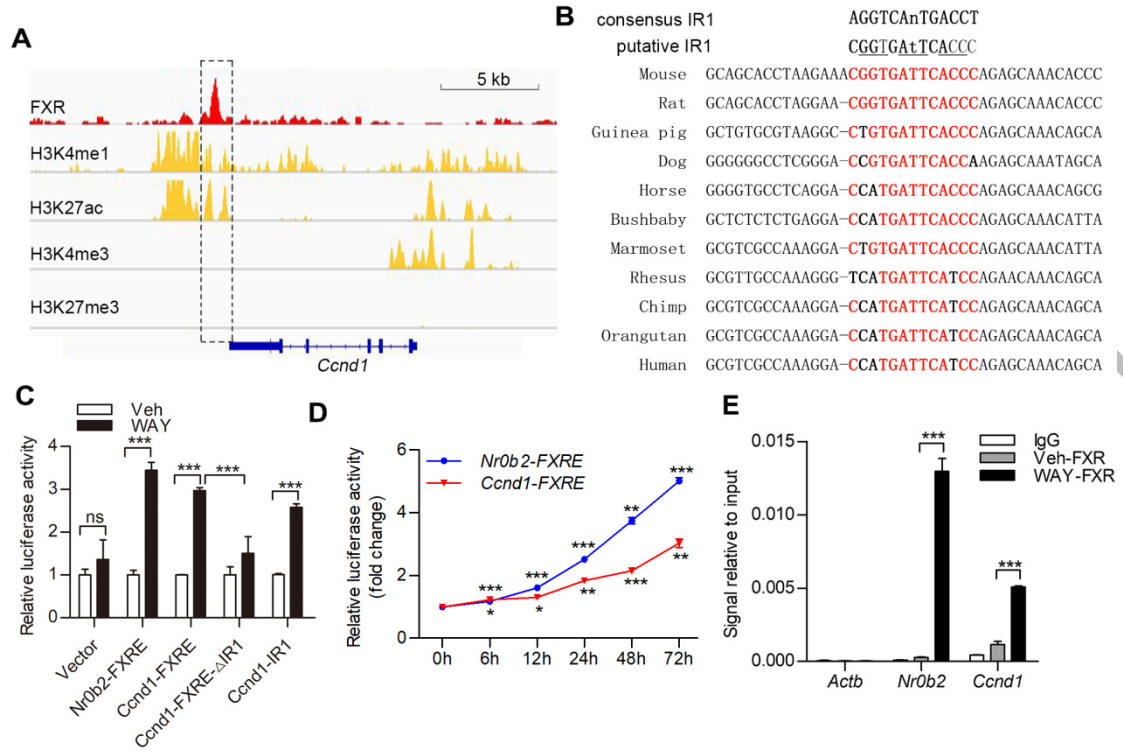


Figure 5

Accepted Manuscript

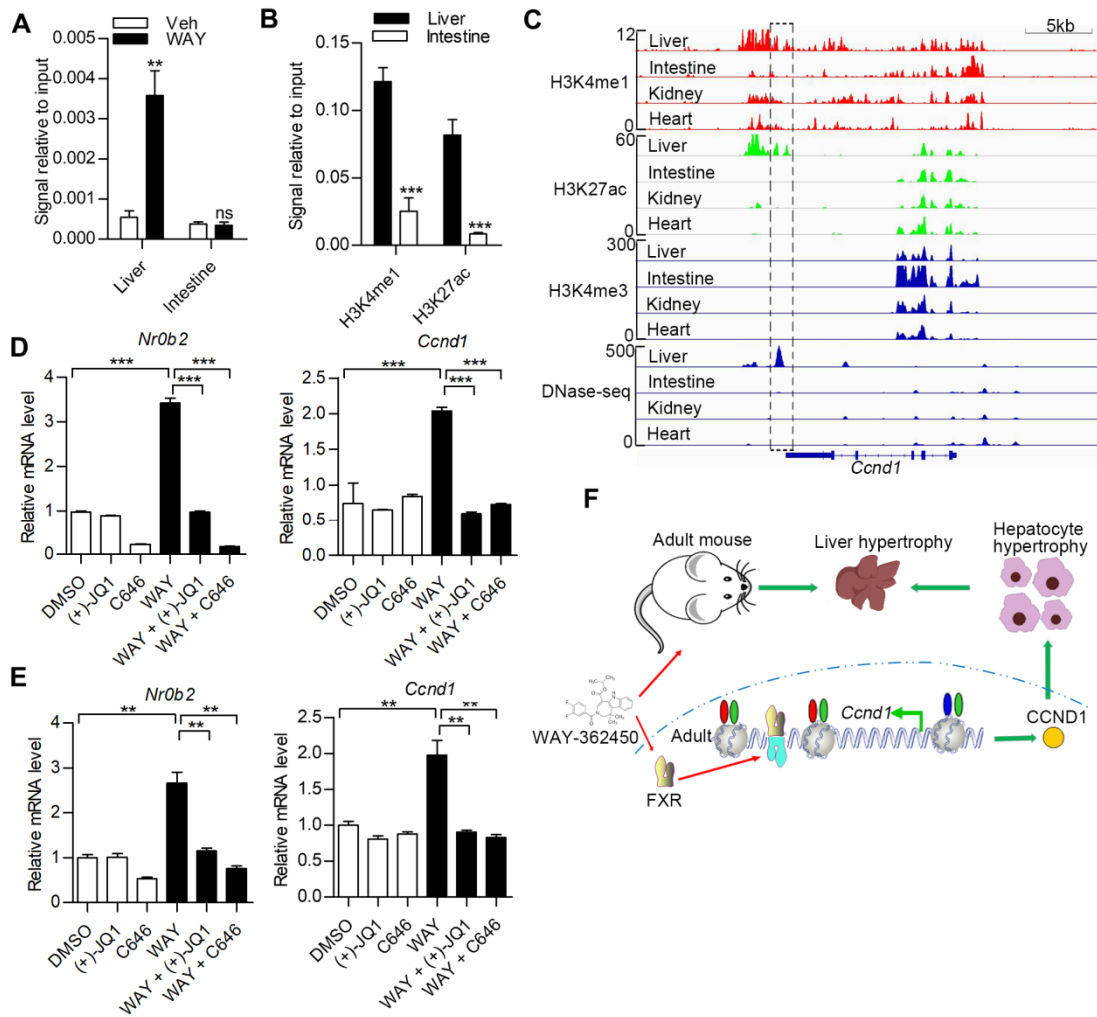


Figure 6

Supplementary material

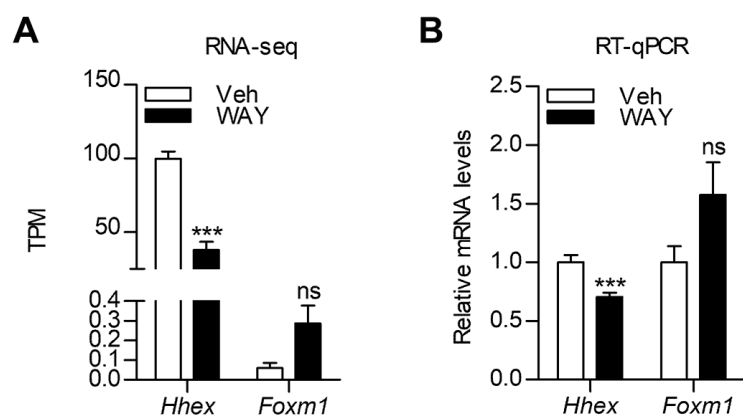


Figure S1. Effect of WAY-362450 on the expression of *Hhex* and *Foxm1*. (A) Transcripts per million (TPM) for *Hhex* and *Foxm1* genes in RNA-seq result from vehicle (Veh) or WAY-362450 (WAY) treated mice livers were shown (n=3; *** FDR < 0.001, ns: not significant (FDR>0.05)) (B) Liver tissues from mice treated with vehicle or WAY-362450 were subjected to RT-qPCR assays for determination mRNA expression of *Hhex* and *Foxm1* (n=8; ***p < 0.001, ns: not significant (p>0.05)).

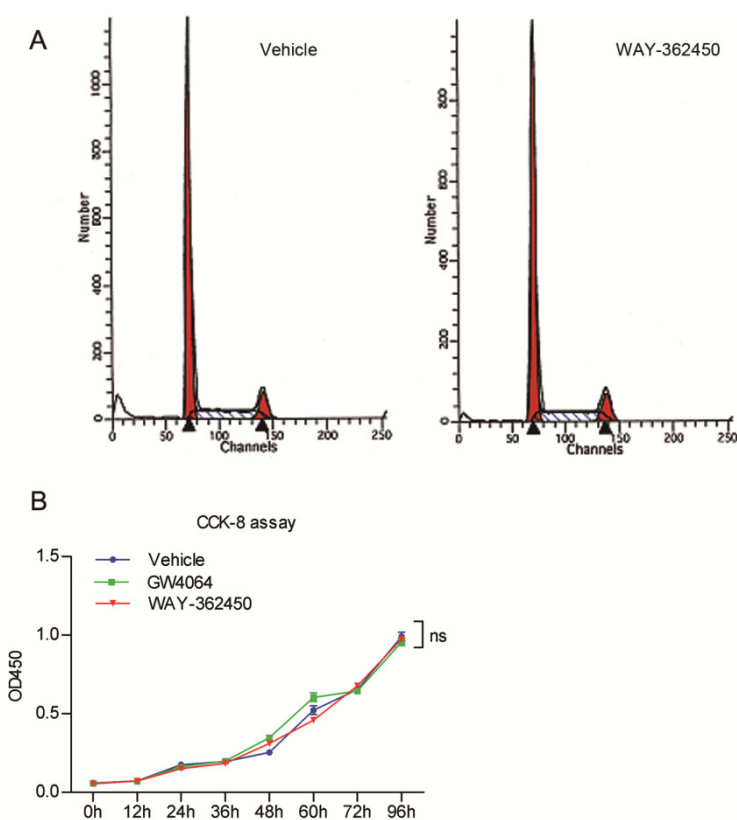


Figure S2. FXR agonist did not affect hepatocyte growth *in vitro*. (A) Cell cycles of mouse primary hepatocyte upon vehicle or WAY-362450 (2 μ M) treatment for 24h was analyzed by flow cytometer. (B) CCK-8 assay for HepG2 cells growth was conducted after treatment with vehicle or WAY-362450 (2 μ M) for the indicated times (n=8, ns, not significant, two-way ANOVA)

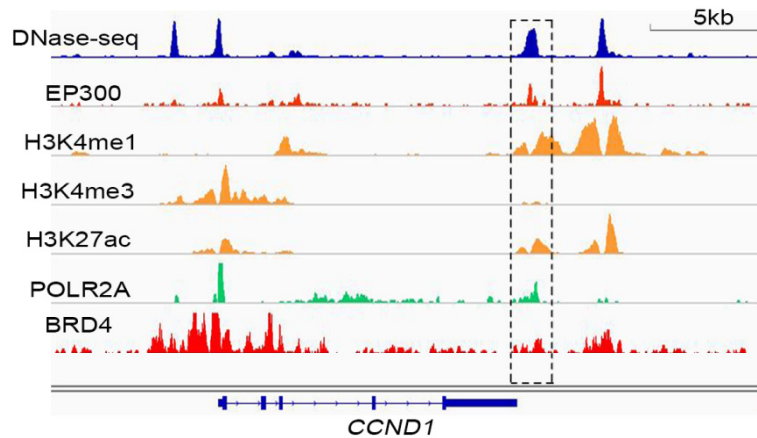


Figure S3. Signature of downstream enhancer of *CCND1* in HepG2 cells. DNase-seq and ChIP-seq (H3K4me1, H3K4me3, H3K27ac, EP300, POLR2A and BRD4) data on HepG2 cell line from ENCODE were subjected to analysis for chromatin accessibility and enhancer signature at *CCND1* downstream region.

Table S1. List of primers for RT-qPCR assay.

Gene symbol (official name)	Alias	Forward Primer	Reverse Primer
For mouse			
<i>Nr0b2</i>	Shp	GGAGTCTTTCTGGAG CCTTGAG	GCACATCTGGGTTGAA GAGGAT
<i>Abcb11</i>	Bsep	TCTGACTCAGTGATT CTTCGCA	CCCATAAACATCAGCC AGTTGT
<i>Cyp7a1</i>		AGACCTCCGGGCCTT CCT	ATCACTCGGTAGCAGA AGGCAT
<i>Ccna2</i>	Cyclin A2	TGATGCTTGTCAAATG CTCAGC	AGGTCCTCCTGTACTG CTCAT
<i>Ccnb1</i>	Cyclin B1	TGGATGGCAGTTTTG AATCACC	CCCTAAGGTACGTGTG AATGTC
<i>Ccnb2</i>	Cyclin B2	GGAGTGGCTGTGCCT CGTCCG	ATCACTGGACACCGTC GGGCGT
<i>Ccnd1</i>	Cyclin D1	ATCCGCAAGCATGCA CAGA	GGGTGGGTTGGAAATG AACTT
<i>Ccne1</i>	Cyclin E1	CCGTCTTGAATTGGG GCAATA	GAGCTTATAGACTTCGC ACACC
<i>Cdkn1a</i>	p21Cip1	CGAGAACGGTGGAAC TTTGAC	CCAGGGCTCAGGTAGA CCTT
<i>Cdkn1b</i>	p27Kip1	TCAAACGTGAGAGTG TCTAACG	CCGGGCCGAAGAGATT TCTG
<i>Cdkn2c</i>	p18INK4c	CCTTGGGGGAACGAG TTGG	AAATTGGGATTAGCAC CTCTGAG
<i>Cdk1</i>	Cdc2	AGATCAGACTTGAAA	GCAGGCTGACTATATTT

		GCGAGGA	GGATGT
<i>Cdk2</i>		ATGGAGAACTTCCAA AAGGTGG	CAGTCTCAGTGTGCGAG CCG
<i>Cdk4</i>	Crk3	ATGGCTGCCACTCGAT ATGAA	TCCTCCATTAGGAACTC TCACAC
<i>Cdk6</i>	Crk2	CCTTACCTCGGTGGT CGTC	GAACTTCCACGAAAAA GAGGCT
<i>Ccnd2</i>	Cyclin D2	GGAACCTGGCCGCAG TCACC	CGACGGCGGGTACATG GCAA
<i>Ccnd3</i>	Cyclin D3	ATGCTGGAGGTGTGT GAGGA	CCACAGCCTGGTCCGT ATAG
<i>Mki67</i>	Ki-67	CTCCCAAGGGTTCCT TCAGC	AGGCATTCCCTCACTCT TGT
<i>Pcna</i>		CCTGTGCAAAGAATG GGGTG	AGACAGTGGAGTGGCT TTTGT
<i>Hhex</i>	HEX	CGGACGGTGAACGAC TACAC	CGTTGGAGAACCTCAC TTGAC
<i>Foxm1</i>	FOXM1b	ATCACGGAGACGTTG GGAC	CCACTGGATATTGGTTA AGCTGT
<i>Actb</i>	β -actin	GTGACGTTGACATCC GTAAAGA	GCCGGACTCATCGTAC TCC
For human			
<i>NR0B2</i>	SHP	TGAAGTCCTGGAACC CTGGTG	CCAATGATAGGGCGAA AGAA
<i>CCND1</i>	Cyclin D1	TATTGCGCTGCTACC GTTGA	CCAATAGCAGCAAACA ATGTGAAA
<i>ACTB</i>	β -actin	TTGCGTTACACCCTTT CTTG	GCTGTCACCTTCACCG TTC

Table S2. List of public data re-analyzed in this study.

Description	Data source	Accession number
FXR ChIP-seq for adult mouse liver	GEO dataset (https://www.ncbi.nlm.nih.gov/geo/)	GSE73624
H3K4me1/H3K4me3/H3K27ac/H3K27me3 ChIP-seq on adult mouse liver	ENCODE project (https://www.encodeproject.org/)	ENCSR854HXZ
H3K4me1/H3K27ac/H3K4me3 ChIP-seq on adult mouse small intestine	ENCODE	ENCDO956IXV
H3K4me1/H3K27ac/H3K4me3 ChIP-seq on adult mouse kidney	ENCODE	ENCSR607TSZ
H3K4me1/H3K27ac/H3K4me3 ChIP-seq on	ENCODE	ENCSR656TAD

adult mouse heart		
DNase-seq on adult mouse liver/intestine/kidney/heart	GEO	GSE37074
H3K4me1/H3K27ac/H3K4me3/EP300/POLR2A/DNase-seq/ BRD4 ChIP-seq on human HepG2 cell line	ENCODE	ENCSR888GEN, ENCSR000EJV, ENCSR514EOE

Table S3. List of primary antibodies used for Western blotting (WB), immunohistochemistry (IHC), immunofluorescence (IF) and chromatin immunoprecipitation (ChIP) assays in this study

Antibody	Manufacturer	Application
Rabbit anti- β -Actin	Abmart Inc., Shanghai, China	WB (1:5000)
Rabbit anti-cyclin D1	Santa Cruz Biotechnology, Santa Cruz, CA, USA	WB (1:1000), IHC (1:50)
Rabbit anti-Ki67	Cell Signaling Technology, Danvers, MA, USA	IHC (1:200)
Rabbit anti-p-H3(ser10)	Cell Signaling Technology, Danvers, MA, USA	IHC (1:200)
Rabbit anti-pan-Cadherin	Cell Signaling Technology, Danvers, MA, USA	IF (1:100)
Rabbit anti-FXR	Santa Cruz Biotechnology, Santa Cruz, CA, USA	ChIP (1:50)
Rabbit anti-H3K4me1	Cell Signaling Technology, Danvers, MA, USA	ChIP (1:50)
Rabbit anti-H3k27ac	Cell Signaling Technology, Danvers, MA, USA	ChIP (1:100)